



AUTHOR(S):

TITLE:

YEAR:

Publisher citation:

OpenAIR citation:

Publisher copyright statement:

This is the _____ version of an article originally published by _____
in _____
(ISSN _____; eISSN _____).

OpenAIR takedown statement:

Section 6 of the "Repository policy for OpenAIR @ RGU" (available from <http://www.rgu.ac.uk/staff-and-current-students/library/library-policies/repository-policies>) provides guidance on the criteria under which RGU will consider withdrawing material from OpenAIR. If you believe that this item is subject to any of these criteria, or for any other reason should not be held on OpenAIR, then please contact openair-help@rgu.ac.uk with the details of the item and the nature of your complaint.

This publication is distributed under a CC _____ license.

Manuscript Number: POWER-D-18-03495R1

Title: A Green and Template-free Synthesis Process of Superior Carbon Material with Ellipsoidal Structure as Enhanced Material for Supercapacitors

Article Type: Research Paper

Keywords: 3D materials; Porous carbon; Supercapacitor; Template free; Metal organic frameworks

Corresponding Author: Professor Junqing Pan, Ph.D

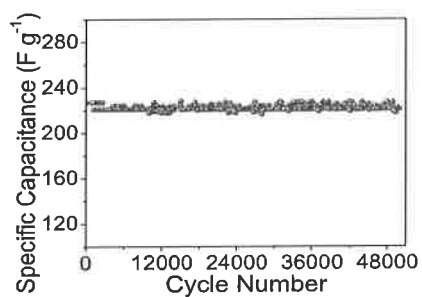
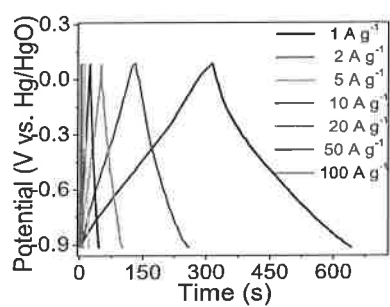
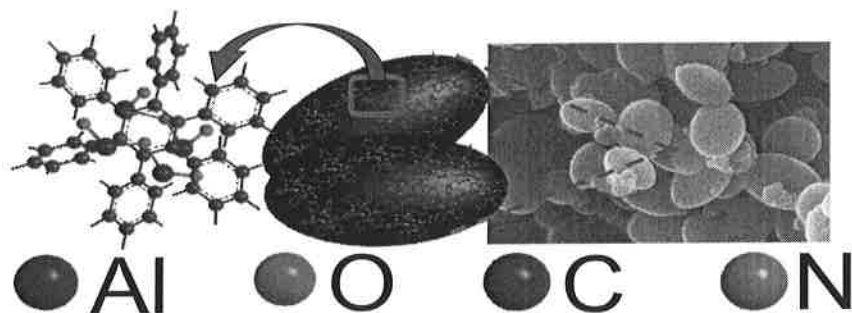
Corresponding Author's Institution: Beijing University of Chemical Technology

First Author: Yanzhi Sun

Order of Authors: Yanzhi Sun; Shicheng Guo; Wei Li; Junqing Pan, Ph.D; Carlos Fernandez; Raja Arumugam Senthil; Xueliang Sun

Abstract: Metal Organic Frameworks (MOF) or related carbon materials are the ideal materials for supercapacitors (SPs) due to their high surface area and unique porous structure. Here, we propose a new green and recyclable synthesis method of porous carbon (PC). Aluminum hydroxide ($\text{Al}(\text{OH})_3$) and trimesic acid (BTC) are employed as raw materials to obtain aluminium trimesic (denoted as Al-BTC) via their covalent reaction, then the PC is obtained through carbonization and dissolving process to remove the aluminum oxide (Al_2O_3). $\text{Al}(\text{OH})_3$ is recovered by the Bayer method for the next batch. The SEM images show that the PCs have rugby-like morphology with the same of 400 nm wide and 1000 nm long which indicates the PC with c/a ratio of 2.5 providing the largest specific volume surface area. The sample offers 306.4 F g^{-1} at 1 A g^{-1} , and it can retain 72.2% even at the current density of 50 A g^{-1} . In addition, the PC provides excellent durability of 50,000 cycles at 50 A g^{-1} with only 5.05% decline of capacitance. Moreover, the PC has an ultrafast charge acceptance, and only 4.4 s is required for one single process, which is promising for application in electric vehicles.

Graphical Abstract



Highlights

1. The ellipsoid-like porous carbon material is prepared with a template-free method.
2. The raw material $\text{Al}(\text{OH})_3$ can be recovered from a hydrolysis process of Bayer method.
3. The obtained carbon material shows excellent electrochemical performance.

1
2
3 **A Green and Template-free Synthesis Process of Superior Carbon Material**
4 **with Ellipsoidal Structure as Enhanced Material for Supercapacitors**
5

6 Yanzhi Sun^a, Shicheng Guo^a, Wei Li^b, Junqing Pan^{a,*}, Carlos Fernandez^c, Raja Arumugam
7
8 Senthil^a, Xueliang Sun^{d,*}
9

10
11
12
13
14 *^aState Key Laboratory of Chemical Resource Engineering, Beijing Engineering Center for*
15 *Hierarchical Catalysts, Beijing Advanced Innovation Center for Soft Matter Science and*
16 *Engineering, Beijing University of Chemical Technology, Beijing 100029, China.*

17
18
19
20
21 *^bDepartment of Engineering Technology and Texas Center for Superconductivity, University*
22 *of Houston, Houston, TX 77204, USA.*

23
24
25
26 *^cSchool of Pharmacy and Life Sciences, Robert Gordon University, Aberdeen, AB10 7GJ, UK.*

27
28
29
30
31 *^dDepartment of Mechanical and Materials Engineering, University of Western Ontario,*
32 *London, ON N6A 5B9, Canada.*

33
34
35
36
37
38
39
40
41
42
43
44
45
46
47
48
49
50
51
52
53
54
55
56
57
58 * Corresponding author: Tel./Fax: +86-10-64448461 (J. Pan)

59
60 E-mails: jqpan@mail.buct.edu.cn (Junqing Pan) & xsun9@uwo.ca (Xueliang Sun)

Abstract

1
2
3
4
5
6
7
8
9
10
11
12
13
14
15
16
17
18
19
20
21
22
23
24
25
26
27
28
29
30
31
32
33
34
35
36
37
38
39
40
41
42
43
44
45
46
47
48
49
50
51
52
53
54
55
56
57
58
59
60
61
62
63
64
65

Metal Organic Frameworks or related carbon materials are the ideal materials for supercapacitors due to their high surface area and unique porous structure. Here, we propose a new green and recyclable synthesis method of porous carbon. Aluminum hydroxide ($\text{Al}(\text{OH})_3$) and trimesic acid (BTC) are employed as raw materials to obtain aluminium trimesic (denoted as Al-BTC) via their covalent reaction. Then, the porous carbon is obtained through carbonization and dissolving process to remove the aluminum oxide (Al_2O_3). $\text{Al}(\text{OH})_3$ is recovered by the Bayer method for the next batch. The SEM images show that the porous carbon has rugby-like morphology with the same of 400 nm wide and 1000 nm long which indicates the porous carbon with c/a ratio of 2.5 providing the largest specific volume surface area. The sample offers 306.4 F g^{-1} at 1 A g^{-1} , and it can retain 72.2% even at the current density of 50 A g^{-1} . In addition, the porous carbon provides excellent durability of 50,000 cycles at 50 A g^{-1} with only 5.05% decline of capacitance. Moreover, the porous carbon has an ultrafast charge acceptance, and only 4.4 s is required for one single process, which is promising for application in electric vehicles.

Keywords: 3D Materials, Porous carbon, Supercapacitor, Template free, Metal organic frameworks

1. Introduction

1
2 In order to meet the growing energy demand, a great number of research has focused on
3
4 developing new energy materials with long cycling life for the application in supercapacitors
5
6 (SPs) [1-6]. SPs or electrochemical capacitors with ultrahigh power density and good
7
8 durability are widely used in hybrid electric vehicles (HEV), military space, and biomedical
9
10 equipment, becoming one of the most important energy-storage devices [7-12]. SPs usually
11
12 used the porous carbon (PC) [13], activated carbon [9], graphene [15, 16], and carbon
13
14 nanotubes [17,18] as active materials because of their high chemical stability, large surface
15
16 area, and special nano effects [19].
17
18

19
20 In recent years, carbon materials with 2D structure, such as graphene with large surface area,
21
22 high conductivity, and short ion diffusion distance, have gradually attracted researchers'
23
24 attention [20]. The most effective preparation method for these materials is using graphene
25
26 oxide to prepare 2D interconnected carbon nanosheets with a Brunauer-Emmett-Teller (BET)
27
28 surface area in the range of 1400-2200 m² g⁻¹ [21]. However, the 2D carbon nanosheets may
29
30 easily overlap with each other in the practical electrodes, which drastically reduce the surface
31
32 area and the electrochemical performance [22]. To resolve the overlap problem and further
33
34 enable the SPs to have higher energy densities, various materials with new synthesis methods
35
36 have been proposed [23-30]. However, the dense structure and amorphous morphology limit
37
38 their energy density, power density and durability.
39
40
41
42
43
44

45
46 More recently, metal-organic frameworks (MOFs) have attracted much interests as
47
48 novel types of nanoporous crystalline materials owing to their large surface area, high pore
49
50 volume and tunable morphology with 3D structure [31-34]. MOFs have been fabricated
51
52 through metal-containing nodes in connection with organic ligands and also utilized as active
53
54 materials in different applications, such as gas separation, gas and vapor storage, water
55
56 purification, energy storage device, etc [35,36]. In recent years, the 3D structured PC
57
58
59
60
61
62
63
64
65

1 materials derived from MOF precursor via thermal carbonization in inert atmosphere with
2 large surface area and high porosity have been reported for the application in SPs. For
3 example, Zhang et al. [37] prepared PC from Ni-based MOF with specific surface area of
4 1143 m² g⁻¹ and achieved a specific capacitance of 211 F g⁻¹ at a current density of 1 A g⁻¹.
5
6 Liu et al. [38] developed PC nanosheets using Al-based MOF with a specific capacitance of
7 88 F g⁻¹ at a current density of 1 A g⁻¹ in 6 M KOH electrolyte. Yang et al. [39] derived the
8 PC with large surface area of 2816 m² g⁻¹ and high porosity from Zn-based MOF for SPs and
9 obtained a specific capacitance of 170 F g⁻¹ at current density of 1 A g⁻¹. Xin et al. [33] also
10 synthesized N-doped PC/graphene composite from hierarchical Zn-based MOF for SPs,
11 supplying a high specific capacitance of 245 F g⁻¹ at a current density of 1 A g⁻¹. Yan et al.
12 [34] reported PC from Al-based MOF for SPs, which showed a specific capacitance of 232.8
13 and 173.6 F g⁻¹ at current density of 0.1 and 1 A g⁻¹, respectively. In addition, Zhang et al.
14 [40] prepared the hierarchical PC from Al-based MOF for SPs, which shows a high specific
15 capacitance of 249 F g⁻¹ at a current density of 1 A g⁻¹.

16
17
18
19
20
21
22
23
24
25
26
27
28
29
30
31
32
33
34 The above reports reveal that the surface morphology and pore volume of the carbon
35 materials have significant impact on the electrochemical performance of SPs. Moreover, the
36 combination of mesopores and micropores of PC can enhance the capacitance as the
37 electrolyte solution moves via the mesopores and aslo electrolyte ions are stored in the
38 micropores during the charging/discharging process [37-41]. However, it is found that their
39 uniform 3D morphology is dependent on the addition of template, and their electrochemical
40 performance is dependent on the contained metal ions and the subsequent high temperature
41 carbonization process. These three problems greatly increased the cost of the materials and
42 limited the large-scale application. In addition, recycling of involved chemicals as the next
43 batch's raw materials and designing a metal free materials to decrease the pollution of waste
44 chemicals have never been reported so far.

1
2
3
4
5
6
7
8
9
10
11
12
13
14
15
16
17
18
19
20
21
22
23
24
25
26
27
28
29
30
31
32
33
34
35
36
37
38
39
40
41
42
43
44
45
46
47
48
49
50
51
52
53
54
55
56
57
58
59
60
61
62
63
64
65

Herein, we propose a facile, green and template-free method to prepare PC by the carbonization of rugby-like Al-based MOF, (Al-BTC, $(\text{Al}_2\text{O}(\text{OH})_{18}(\text{H}_2\text{O})_3(\text{Al}_2(\text{OH})_4)(\text{BTC})_6 \cdot 24 \text{H}_2\text{O})$), in which $\text{Al}(\text{OH})_3$ and BTC along with CTAB as an additive are employed as raw materials to prepare hierarchical nano PC. In addition, our proposed methodology presents the advantage of recycling of $\text{Al}(\text{OH})_3$ which is recovered through the hydrolysis process by Bayer method and used as raw material for the next batch. The obtained PC has a high specific surface area of $1,400 \text{ m}^2 \text{ g}^{-1}$ containing both micropores ($< 2 \text{ nm}$) and mesopores ($2\text{-}5 \text{ nm}$). The obtained PC sample offers a superior electrochemical performance for SPs with high specific capacitance of 306.4 F g^{-1} at current density of 1 A g^{-1} , excellent durability of 50,000 cycles at ultrahigh current density of 50 A g^{-1} with only 5.05% decay, and remarkable ultrafast charge acceptance of 4.4 s for one charge process.

2. Experimental Section

2.1. Preparation Al-MOFs and porous carbon

1.651 g aluminum hydroxide (65%, Tianjin Zhiyuan Chemical Reagent Co., Ltd.) mixed with 5 drops of $1 \text{ mol L}^{-1} \text{ HNO}_3$ was dispersed in 30 ml deionized water, marked as solution A. 0.663 g trimesic acid (99%, Guangdong Wengjiang Reagent Co., Ltd.) and 1.812 g cetyltrimethylammonium bromide (CTAB) (99%, Tianjin Jingke Fine Chemical Research Institute) was dissolved in 30 ml ethanol, marked as solution B. Solution A and B were mixed in 100 ml three neck bottle under stirring for 30 min. Then, the mixture was moved to a 100 mL Teflon-lined stainless steel autoclave (100 ml, Zhengzhou Boke Co., Ltd., 304 stainless steel + PTFE) to be heated at $120 \text{ }^\circ\text{C}$ for 9 h. After finishing the reaction, the product was filtered and washed deionized water, and then, obtained Al-BTC was drying in a vacuum oven at $60 \text{ }^\circ\text{C}$ for 12 h. After that, 0.5 g Al-BTC was moved to a nickel boat and carbonized at $800 \text{ }^\circ\text{C}$ for 2 h in a vacuum tube furnace at a heating rate of $5 \text{ }^\circ\text{C min}^{-1}$, followed by natural cooling to room temperature to obtain the C/ Al_2O_3 composite. The C/ Al_2O_3 was dissolved in

1 8 M NaOH-1.2 M NaAl(OH)₄ solution at 120 °C under stirring for 10 min to remove Al₂O₃.

2 The product was filtered and washed with deionized water until the filtrate presented neutral
3
4 to obtain porous carbon (PC).
5
6

7 **2.2. Morphological and Structural Characterizations**

8
9 The morphology and surface structure of synthesized Al-BTC, C/Al₂O₃ and PC
10 samples were characterized by a scanning electron microscope equipped with energy
11 dispersive spectroscopy (SEM/EDX, Zeiss SUPRA 55). The structure of the obtained samples
12 were characterized by X-ray diffraction (XRD) on a Bruker D8 Advance X-Ray
13 Diffractometer using a Cu K α , and the scanning rate was 10° min⁻¹ in the range of scanning
14 angle (2 θ) from 5° to 90°. The high resolution-transmission electron microscopy (HR-TEM)
15 images of samples were collected on a Philips CM200FEG Field Emission Microscope. The
16 Brunauer Emmett Teller (BET) specific surface area, pore volume and pore size distribution
17 of the as-prepared samples were studied using nitrogen adsorption-desorption analysis by a
18 QuandasorbSI model particle analyzer. Thermal gravimetric analysis (TGA) was performed
19 on a NETZSCHSTA 4449F 3STA449F3A-024-M model thermal analyzer in the temperature
20 range from 20 °C to 900 °C under N₂ atmosphere at a heating rate of 10 °C min⁻¹. The X-ray
21 photoelectron spectra (XPS) were performed on a Thermo Fisher ESCALAB 250 X-ray
22 photoelectron spectrometer with monochromated Al K α radiation source.
23
24
25
26
27
28
29
30
31
32
33
34
35
36
37
38
39
40
41
42

43 **2.3. Electrochemical Tests**

44
45 800 mg samples, 200 mg expanded graphite (99.9%, Qingdao Laixi Fine Graphite) and
46 50 mg PTFE (60 wt.%, Guangzhou Songbai Chemicals) were mixed and ground in an agate
47 mortar for 30 min. Then, the obtained paste was rolled into 50 μ m thick as electrode film and
48 cut into the size of 10 mm \times 10 mm, and applied on the of nickel foam of the same size
49 (density: 550 \pm 30 g m⁻², pores per inch: 100 \pm 30, thickness: 1.8 \pm 0.1 mm, purchased from
50 Changsha Liyuan New Materials) to form the composite plate, which was then pressed by a
51
52
53
54
55
56
57
58
59
60
61
62
63
64
65

1 pressing machine (YP-15A, Shanghai Jingsheng Instrument) for 30 s at 10 MPa to obtain
2 working electrode.
3

4 Electrochemical tests were performed by a three electrodes system using 6 M KOH as
5 electrolyte at room temperature. A 10 mm × 10 mm Nickel plate used as auxiliary electrode
6 and a Hg/HgO electrode as reference electrode. The charge/discharge tests were carried out
7 by a LAND CT2001A battery test system (Jinnuo Wuhan Corp, China) at room temperature.
8
9 Cyclic voltammetry tests (CV, scan range: -0.9-0.1 V (Vs. Hg/HgO), scan rate: 1 - 50 mV s⁻¹)
10 were performed on a CS300 cell test system (Wuhan CorrTest Instruments Co., Ltd.).
11
12
13
14
15
16
17
18

19 3. Results and Discussion

20
21 Fig. 1a and b show the schematic diagram of the process step by step from Al(OH)₃ and
22 BTC to the final formation of Al-BTC, C/Al₂O₃, and PC. Fig. 1 a II illustrates that Al-BTC
23 has its own specific structure of rugby-like particle, which depends on the spatial orientation
24 of Al³⁺ and BTC. Fig. 1 a III displays the C/Al₂O₃ composite obtained during the
25 decarboxylation process at 800 °C. Fig. 1 aIV shows a PC after removing Al₂O₃. In the
26 carbonization process of Al-BTC at high temperatures, CO₂ can easily escape from carboxyl
27 functional groups and hence, the carbonized resultants have welldeveloped uniform holes. In
28 addition, the resultant carbon material contains Al₂O₃ nanoparticles owing to the thermal
29 stability of Al₂O₃ materials. To obtain a larger PC surface area, NaOH-NaAl(OH)₄ was used
30 to remove Al₂O₃ particles from obtained carbon material by Bayer process. NaAl(OH)₄
31 solution was obtained by a regeneration process of NaOH-NaAl(OH)₄ solution. Then,
32 Al(OH)₃ can be recycled and used as a raw material for the next preparation of Al-BTC again,
33 thus forming a green preparation process. Fig. 1b shows the green cycling synthesis of Al-
34 BTC using Bayer process. Fig. S1, S2, and S3 illustrate the photographs, SEM images and
35 XRD patterns, respectively, in which (a) Al(OH)₃ is the raw materials and (b) is the recovered
36 Al(OH)₃ from Bayer process.
37
38
39
40
41
42
43
44
45
46
47
48
49
50
51
52
53
54
55
56
57
58
59
60
61
62
63
64
65

1
2
3
4
5
6
7
8
9
10
11
12
13
14
15
16
17
18
19
20
21
22
23
24
25
26
27
28
29
30
31
32
33
34
35
36
37
38
39
40
41
42
43
44
45
46
47
48
49
50
51
52
53
54
55
56
57
58
59
60
61
62
63
64
65

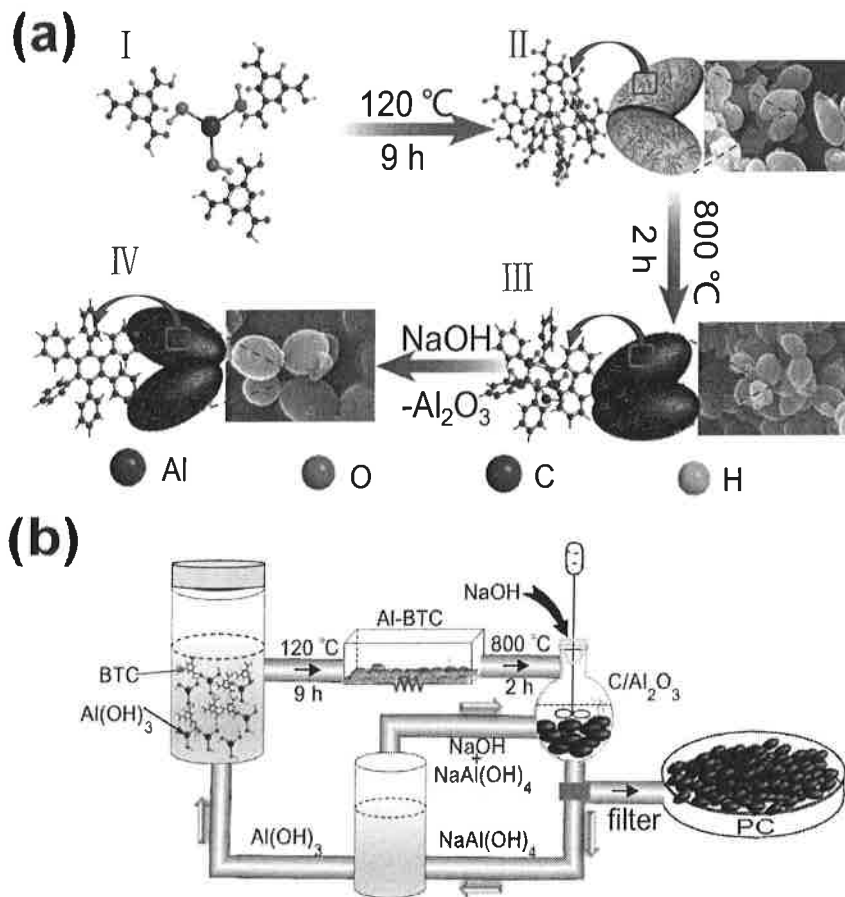


Fig. 1 (a) Diagram from rugby-like Al-BTC to rugby-like PC and (b) diagram of preparation route of PC.

Fig. 2a, b and c show the SEM and element mapping images of the obtained Al-BTC, C/Al₂O₃ composite and PC, respectively. As seen from Fig. 2a, Al-BTC exhibits a typical rugby-like structure, with the average size of particles found to be circa 400 nm in width and 1000 nm in length. Fig. 2b displays that the morphology of C/Al₂O₃ composite retains uniform rugby-like surface, and the surface becomes slightly rough after the carbonation process. This could be attributed to the emission of gases like H₂O, CO or CO₂ during the thermal decomposition process. Fig. 2c shows the obtained PC by dissolving the Al₂O₃ from C/Al₂O₃ composite into a NaOH-NaAl(OH)₄ solution by Bayer method. The PC still retains

1
2
3
4
5
6
7
8
9
10
11
12
13
14
15
16
17
18
19
20
21
22
23
24
25
26
27
28
29
30
31
32
33
34
35
36
37
38
39
40
41
42
43
44
45
46
47
48
49
50
51
52
53
54
55
56
57
58
59
60
61
62
63
64
65

its rugby-like 3D structure, indicating that the morphology of the product is very stable in the alkaline media, even in concentrated NaOH solution. C, Al and O elements can be observed in Fig. 2a and 2b before NaOH treatment. However, after NaOH treatment shown in Fig. 2c, Al and O elements almost disappear, revealing the successful removal of Al_2O_3 by NaOH treatment.

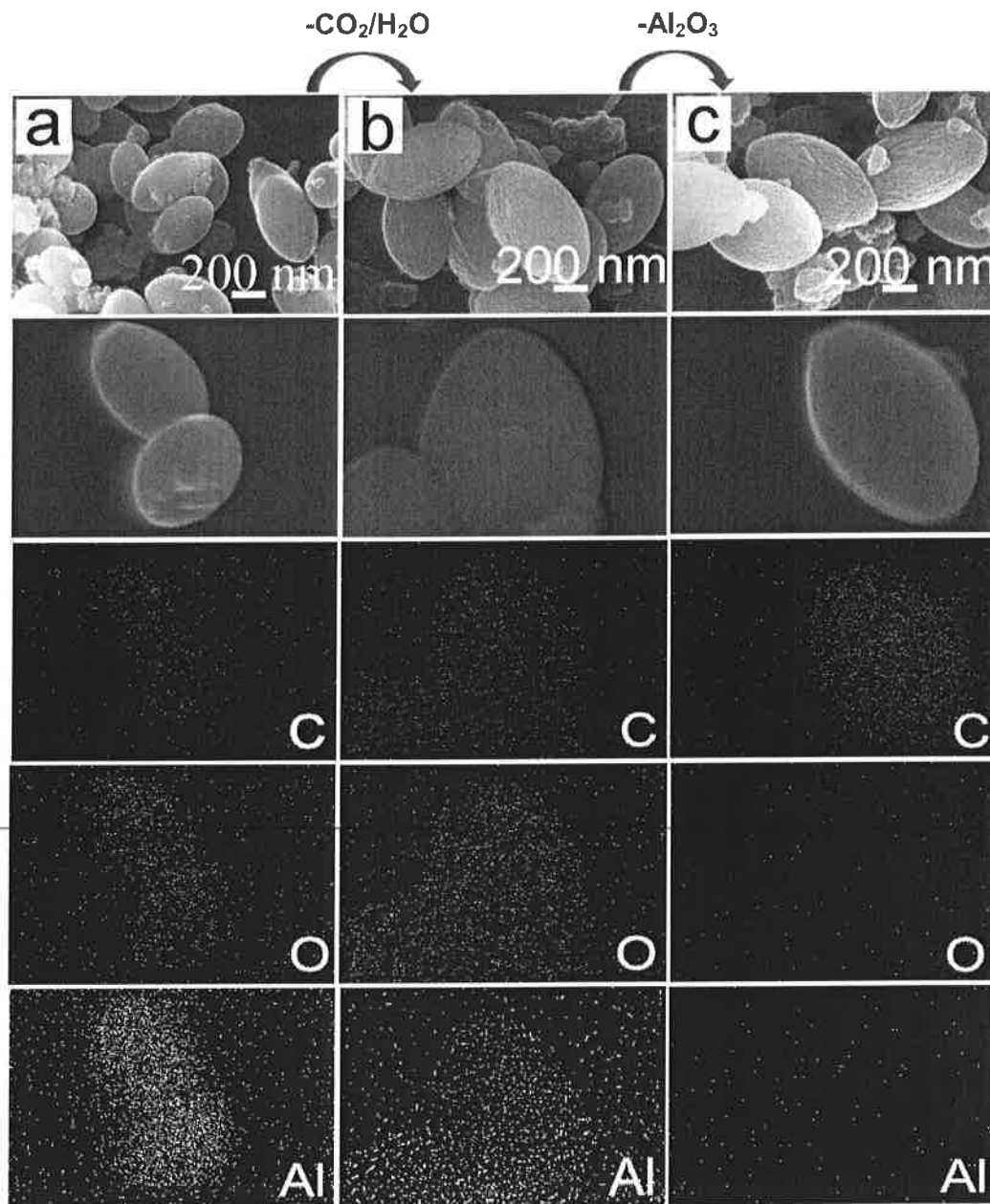


Fig. 2. SEM and mapping images of (a) Al-BTC synthesized at 120 °C for 9 h, (b) C/ Al_2O_3 composite obtained by carbonizing Al-BTC under vacuum at 800 °C for 2 h and (c) PC

1
2
3
4
5
6
7
8
9
10
11
12
13
14
15
16
17
18
19
20
21
22
23
24
25
26
27
28
29
30
31
32
33
34
35
36
37
38
39
40
41
42
43
44
45
46
47
48
49
50
51
52
53
54
55
56
57
58
59
60
61
62
63
64
65

obtained by dissolving sample b in NaOH- NaAl(OH)₄ solution under 120 °C and stirring for 10 min.

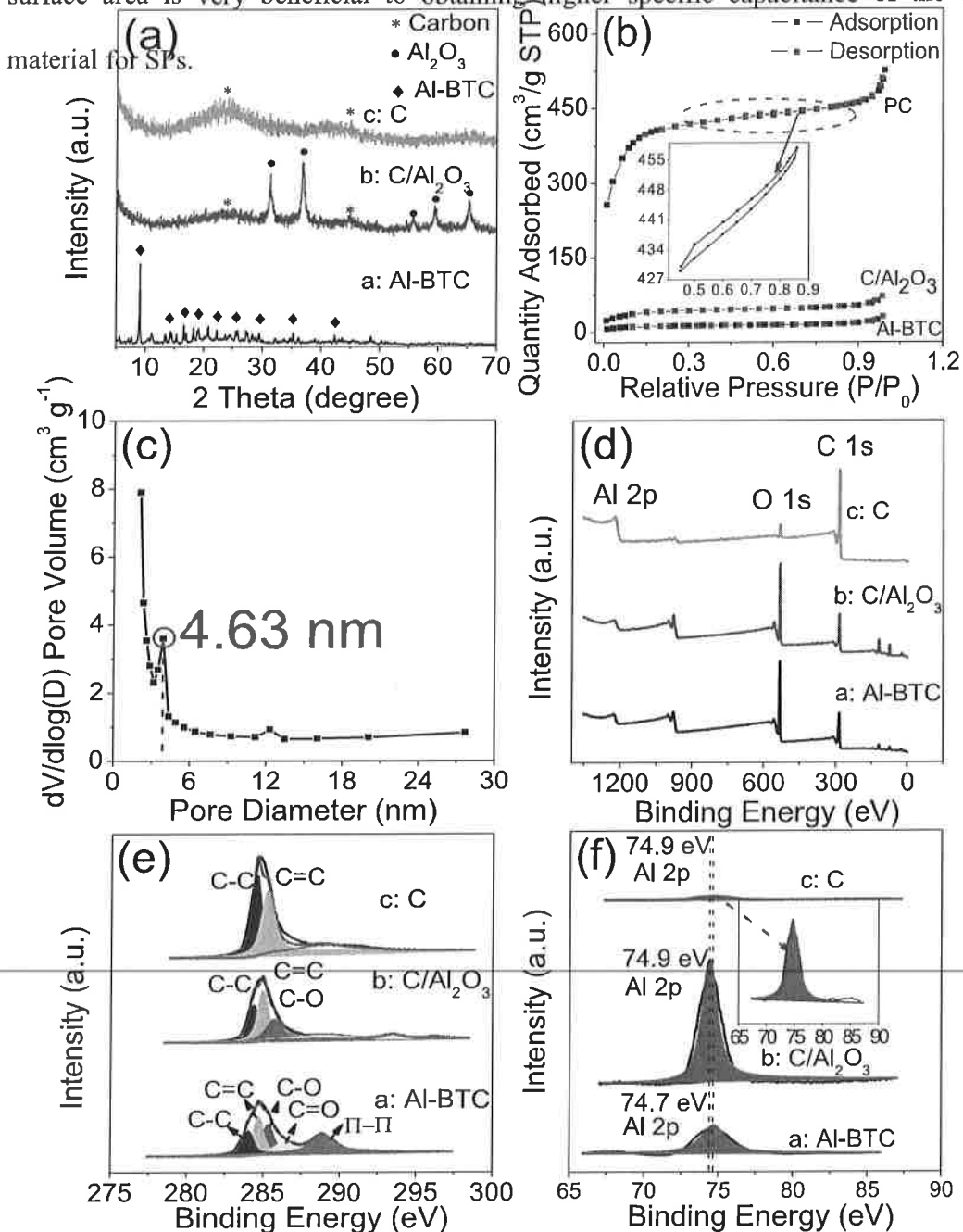
Fig. S4 indicates the TGA curve of the obtained Al-BTC from 20 to 900 °C at heating rate of 10 °C min⁻¹ in N₂ atmosphere. The results show that the Al-BTC begins to form the carbon skeleton and Al₂O₃ during the carbonization process from 500-900 °C. The mass loss in this process is circa 30% which is very close to the calculated value by the decomposition reaction from Al-BTC to C/Al₂O₃ composite. The photographs of the obtained Al-BTC, C/Al₂O₃ and PC are shown in Fig. S5. Fig. S6 and S7 show SEM images of Al-BTC samples obtained at different time and temperatures, respectively. Fig. S8 provides the charge and discharge curves of the obtained PC. The results show that the PC provides the highest electrochemical performance under the optimal preparation conditions of 120 °C for 9 h and carbonization conditions of 800 °C for 2 h, respectively.

Fig. 3a displays the XRD patterns of the obtained Al-BTC, C/Al₂O₃ composite and PC. The XRD pattern of Al-BTC basically conforms to those characteristic peaks of the Al-BTC reported in the literature [42]. The composite of C/Al₂O₃ sample exhibits two broad diffraction peaks at about $2\theta = 25^\circ$ and 45° , which are related to (002) and (101) diffraction planes of porous carbon (JCPDS No. 41-1487), respectively. And also several sharp diffraction peaks appear at $2\theta = 31.83^\circ, 37.55^\circ, 56.72^\circ, 60.49^\circ$ and 66.46° , which can be indexed to (220), (311), (422), (511) and (440) diffraction planes of the Al₂O₃ (JCPDS No. 47-1292), respectively. These diffraction peaks are in good agreement with the earlier reports on Al₂O₃ [43] and carbon [44] in literatures, indicating the composite contains the amorphous carbon and crystallized Al₂O₃. The PC exhibits only two broad diffraction peaks at about $2\theta = 25^\circ$ and 45° , indicating the successful removal of Al₂O₃ nanoparticles by Bayer process and the achievement of a high purity PC material. Fig. 3b shows the BET test results

1 of Al-BTC, C/Al₂O₃ composite and PC. The specific surface areas of the three materials are
2 found to be 45.2, 146.1 and 1400 m² g⁻¹, indicating that the process of decarboxylation and
3 carbonization, especially the subsequent dissolution of Al₂O₃, can greatly improve the carbon
4 surface area. In addition, the carboxyl groups and Al₂O₃ are the natural pore forming agents.
5 Fig. 3d, e, and f show the overview XPS spectra of C 1s and Al 2p of Al-BTC, the composite
6 of C/Al₂O₃ and the PC. As seen from Fig. 3d, the peak intensities of C, O, and Al decrease,
7 which is well consistent with the previous element mapping and XRD results. Fig. 3e shows
8 the detailed XPS spectra of C 1s after peak separation. The peaks of carbon element of Al-
9 BTC at 284.2, 284.6, 285.3, 287.1 eV, correspond to the following bonds: C=C, C-C, C-O,
10 and C=O, respectively. The peak situated at 290.6 eV is attributed to the π - π^* electronic
11 transitions. The peaks of carbon element of C/Al₂O₃ at 284.6 eV correspond to C 1s.
12 Furthermore, the peaks of carbon located at 284.8 eV correspond to C 1s. Fig. 3f shows the
13 detailed XPS spectra of Al 2p after peak separation. The peaks of aluminum found in the
14 following compounds: Al-BTC, C/Al₂O₃ and C at 74.7, 74.9, 74.9 eV, correspond to Al 2p.
15 The bonding of Al in Al-BTC belongs to the functional group -COO-Al, which is different to
16 that in C/Al₂O₃. Therefore, the peaks of aluminum in Al-BTC is different to that of C/Al₂O₃.
17 Moreover, the observed very low intensity of Al peaks in the PC sample indicates the trace
18 Al₂O₃ in the obtained PC.

19 Fig. 4 illustrates the HR-TEM images of the obtained Al-BTC, C/Al₂O₃ and PC under
20 different magnifications. The inserted image of Fig. 4c exhibits the SAED patterns of C/Al₂O₃,
21 in which the diffraction rings clearly reflect the diffraction spots, corresponding to the crystals
22 planes of (220), (311) and (440) of γ -Al₂O₃. The inserted HR-TEM image (Fig. 4d) displays
23 legible lattices fringes in which the adjacent lattices are 0.268 nm and 0.220 nm,
24 corresponding to the (220) and (311) planes of γ -Al₂O₃, respectively, which match the results
25 from the XRD pattern. The nano particles size of γ -Al₂O₃ is 4.64 nm are very close to the size
26 of the hole (4.63 nm) tested by BET. As observed from Fig. 4e and f, after adding

concentrated NaOH (8 M) solution a significant number of holes appear due to removing the nano Al₂O₃ particles, leading to a considerable increase in surface area of the PC. The larger surface area is very beneficial to obtaining higher specific capacitance of the electrode material for SPs.



1
2
3
4
5
6
7
8
9
10
11
12
13
14
15
16
17
18
19
20
21
22
23
24
25
26
27
28
29
30
31
32
33
34
35
36
37
38
39
40
41
42
43
44
45
46
47
48
49
50
51
52
53
54
55
56
57
58
59
60
61
62
63
64
65

Fig. 3 (a) XRD patterns of Al-BTC, C/Al₂O₃ and PC, (b) N₂ adsorption-desorption isotherms curves, (c) pore size distribution of the obtained carbon and (d), (e) and (f) overview of XPS spectra, C 1s spectra and Al 2p spectra of Al-BTC, C/Al₂O₃ and PC, respectively.

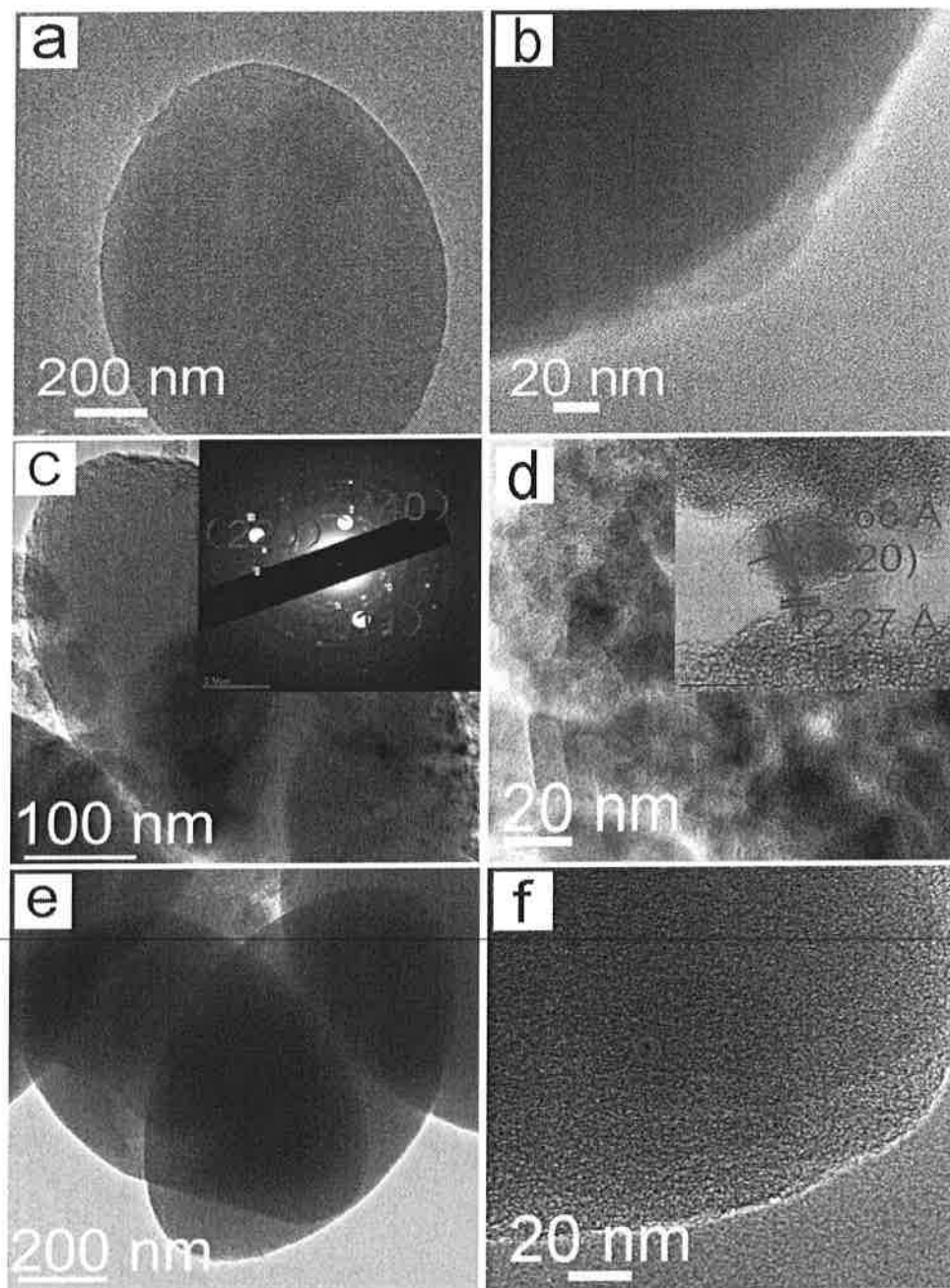


Fig. 4 Different magnification HR-TEM images of (a,b) Al-BTC, (c,d) C/Al₂O₃ and (e,f) PC.

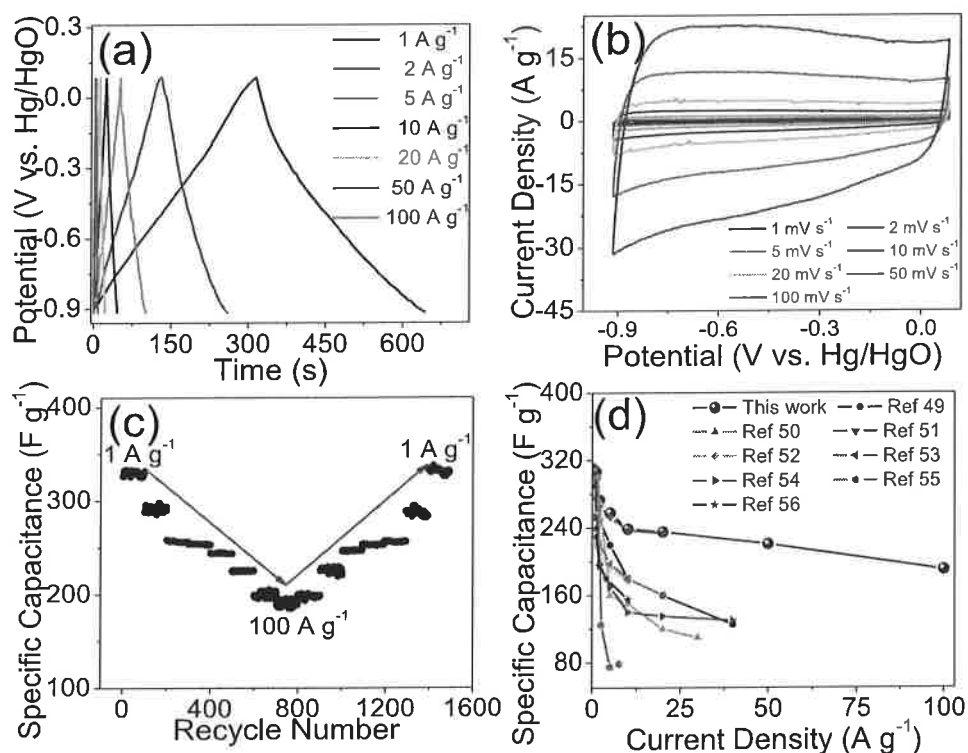
1
2
3
4
5
6
7
8
9
10
11
12
13
14
15
16
17
18
19
20
21
22
23
24
25
26
27
28
29
30
31
32
33
34
35
36
37
38
39
40
41
42
43
44
45
46
47
48
49
50
51
52
53
54
55
56
57
58
59
60
61
62
63
64
65

Fig. 5a illustrates GCD curves of PC under different current densities from 0.5 A g⁻¹ to 100 A g⁻¹ in 6 M KOH electrolyte. In addition, the GCD curves present isosceles triangular shapes in the working voltage range from -0.9 to 0.1 V, indicating that the PC has typical capacitance properties during charge and discharge cycles. By increasing the current density from 1 A g⁻¹ to 100 A g⁻¹, the charge time is greatly reduced from 610 s to 4.4 s, and 72.1% of 306.4 F g⁻¹ is still remained under the ultrahigh current density, reflecting an excellent rate property of PC. The carbon offers significant high charge speed, and only 4.4 s is required for one process, which is suitable for potential applications in electric vehicles.

Fig. 5b displays CV curves of the obtained PC at different scan rates in 6 M KOH. The CV present approximately rectangular shapes without obvious redox peaks, indicating the typical charge/discharge process of double-layer capacitance. The current is raised very fast by increasing the scan rate, showing that the carbon has a rapid response ability. Fig. 5c illustrates the rate performances of the obtained PC at different current densities. The as-prepared PC electrodes were charged/discharged at various current densities of 1, 2, 5, 10, 20, 50, 80 and 100 A g⁻¹ for 100 cycles per step, totally 15 steps. The observed specific capacitances were found to be 303.8, 273.4, 257.6, 254.2, 244.1, 226.1, 198.5 and 190.4 F g⁻¹, respectively. It is important that when the current density is ultra-high, up to 100 A g⁻¹, the reversible capacitance still retains 190.4 F g⁻¹, which is circa 62.7% of that for 1 A g⁻¹, indicating an excellent rate performance. In particular, when the current density is decreased from 100 A g⁻¹ to initial value of 1 A g⁻¹, the capacitance recovers to 299.2 F g⁻¹, which is approximately 98.5% of the initial value after 1,500 cycles, exhibiting superior reversibility against cycling.

Recently, several research groups have reported some 3D PC and nitrogen-doped PC with high specific capacitance and long life [33, 34, 37-40, 45-56]. The electrochemical properties of these materials and the as-prepared PCs are compared in Fig. 5d and Table S1. The PC synthesized in this work provides superior capacitance and excellent rate properties as

1 compared with the reported materials, indicating that the obtained PC is an outstanding active
 2 material for SPs. The prepared PC has shown remarkable electrochemical properties at
 3 ultrahigh current density, which will be very useful in power sources of electric vehicles.
 4
 5 These properties are attributed to its ellipsoidal structure and natural porous structure.
 6
 7
 8
 9
 10
 11
 12
 13
 14
 15
 16
 17
 18
 19
 20
 21
 22
 23
 24
 25
 26
 27
 28
 29
 30
 31
 32
 33
 34
 35
 36
 37
 38
 39
 40
 41



42 **Fig. 5** (a) GCD curves of PC at different current densities from 1-100 A g⁻¹ in 6 M KOH, (b)
 43 CV curves of the PC at different scan rates from 1-100 mV s⁻¹ in the range from -0.9 to 0.1 V
 44 (vs. Hg/HgO) in 6 M KOH at 298 K, (c) SCs cycling properties of the PC at various current
 45 densities, and (d) SCs of the obtained carbon as compared with the other carbons reported in
 46 literature at different current densities.
 47
 48
 49
 50
 51

52 In order to prove that the ellipsoidal structure is beneficial to improving the
 53 electromhemical performance at high current density, we calculate the specific volume
 54 surface area versus different structures. Fig. 6 shows a schematic diagram of different
 55 surface area versus different structures. Fig. 6 shows a schematic diagram of different
 56 structures of 2D materials such as: spherical and ellipsoid with different ratio of polar radius
 57
 58
 59
 60
 61
 62
 63
 64
 65

(c) and equatorial radius (a). The effective area of 2D materials decreases through an overlap of each other. For spherical or ellipsoid materials, their spherical or oval-shaped profiles will effectively minimize the loss of electrochemical reaction surface area. In general, the spherical material can be considered as special case of $c : a = 1 : 1$. In addition, Fig. 6 displays the effective specific surface areas versus different $c : a$ values. The largest specific surface area is obtained when the $c : a$ value is 2.5: 1 on the basis of the same volume. The results of HR-TEM and SEM images show that the obtained PC material has a length of 900-1,000 nm and a width of 350-400 nm, so its $c : a$ value is close to its optical $c : a$ value of 2.5. Therefore, due to this property, the obtained PC material have superior ultrahigh charge and discharge speed compared to other carbon materials reported in literature [50, 53-61].

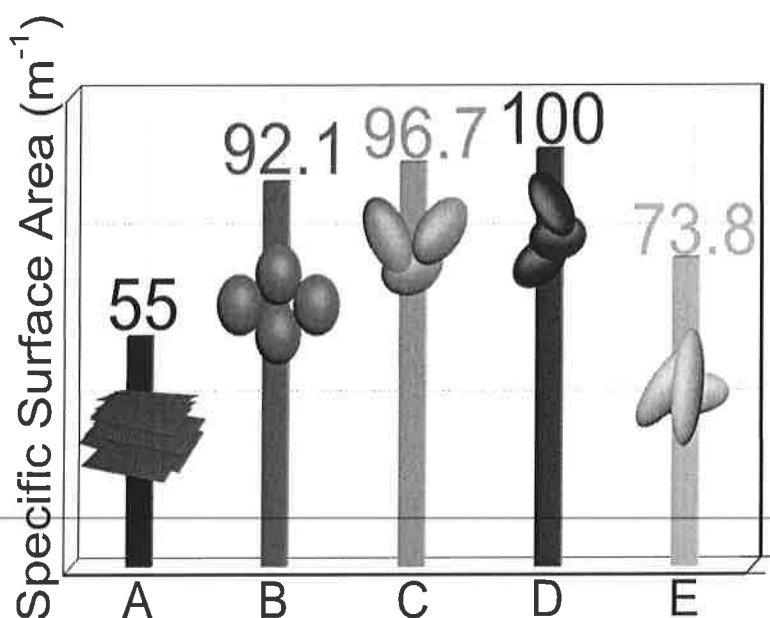


Fig. 6 Diagram of 2D, spherical and ellipsoidal materials at different ratios of polar radius (c) and equatorial radius (a); A: 2 D material, B: Ball ($c : a=1:1$), C: Ellipsoid ($c : a=2:1$), D: carbon of this work ($c : a=2.5:1$) and E: Ellipsoid ($c : a=3:1$).

Fig. 7a and b show SEM images of the obtained PC before and after 50000 cycles. The PC structure in Fig. 7b almost keeps the initial morphology on its surface after 50,000 cycles

1 compared to Fig. 7a. Fig. 7c shows the cycling stability of the PC for 50,000 cycles at the
 2 ultrahigh current density of 50 A g^{-1} . The obtained PC provides excellent durability with very
 3 slight decay of 5.05% after the 50,000 cycles, which is remarkably superior to the existing
 4 materials reported in literature [54-60]. Fig. 7d shows the cycling life of the PC and other
 5 carbons reported in literature [50, 53-61]. It can be seen that the cycling number and
 6 capacitance retention ratio are much higher than those in the reported papers.
 7
 8
 9
 10
 11
 12
 13
 14
 15
 16
 17
 18
 19
 20
 21
 22
 23
 24
 25
 26
 27
 28
 29
 30
 31

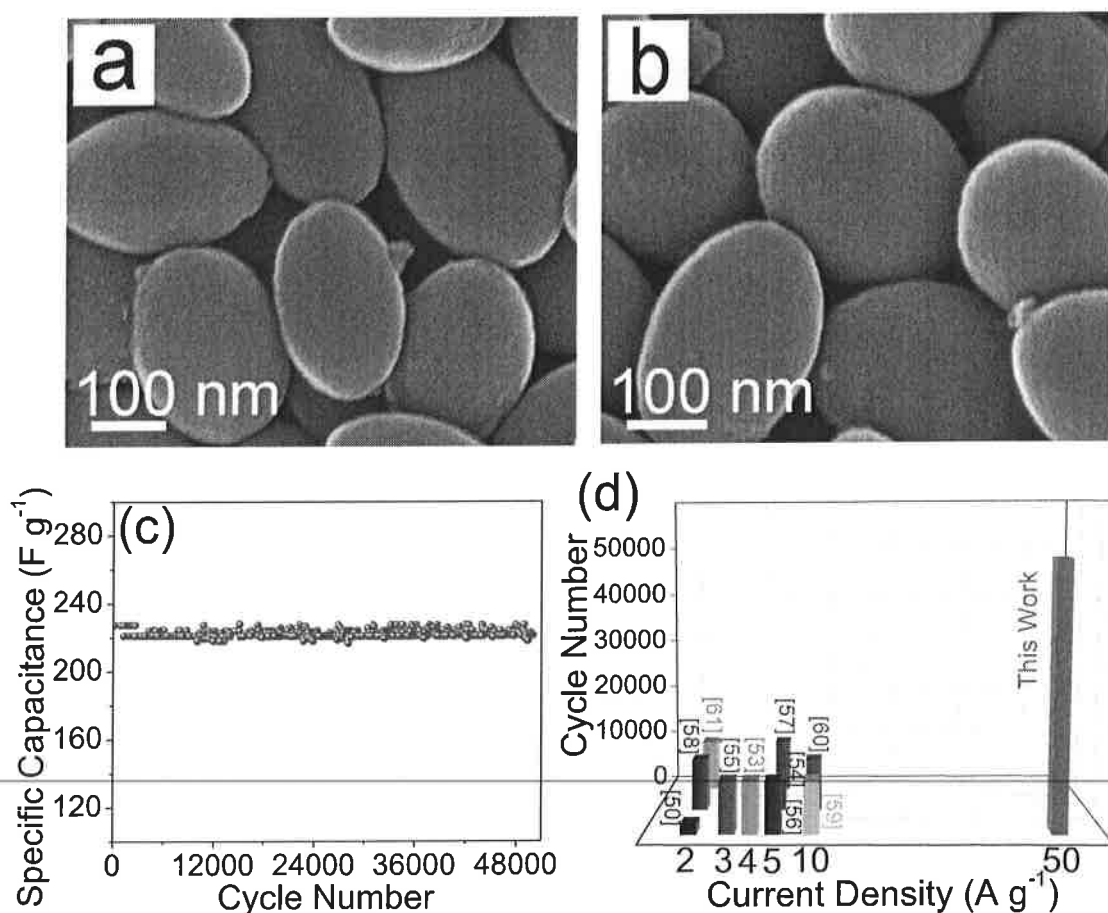


Fig. 7 SEM images of the obtained PC (a) before and (b) after 50,000 cycles, (c) SC curve of the obtained PC after the 50,000 charge and discharge cycles at 50 A g^{-1} in 6 M KOH and (d) the cycling life of the obtained PC and the other PC reported in literatures.

4. Conclusions

In conclusions, $\text{Al}(\text{OH})_3$ and BTC are employed as raw materials to obtain Al-BTC and further produce $\text{C}/\text{Al}_2\text{O}_3$ by carbonation. PC is finally obtained by removing the Al_2O_3 from

1
2
3
4
5
6
7
8
9
10
11
12
13
14
15
16
17
18
19
20
21
22
23
24
25
26
27
28
29
30
31
32
33
34
35
36
37
38
39
40
41
42
43
44
45
46
47
48
49
50
51
52
53
54
55
56
57
58
59
60
61
62
63
64
65

C/Al₂O₃ via the green approach. The beauty of the described methodology is that Al(OH)₃ can be recovered by the Bayer method for the next batch. The bonds of Al-O and carboxyl in Al-BTC are formed of natural pore agent. The specific surface area and pore volume of the rugby-like carbon are found to be 1,400 m² g⁻¹ and 1.172 cm³ g⁻¹, respectively. The PC offers excellent electrochemical performance due to its special structure (axis c/a ratio of 2.5). In addition, it has a specific capacitance up to 306.4 F g⁻¹ at current density of 1 A g⁻¹ and only 72.1% attenuation is observed when the current density increases from 1 A g⁻¹ to 100 A g⁻¹. Furthermore, it has an excellent durability with only 5.05% decay after 50,000 cycles at current density of 50 A g⁻¹. Finally, it offers an ultra-high charge speed, which can finish a charge process for only 4.4 s which is very suitable for potential application in electric vehicles.

Acknowledgements

This work was supported by the National Natural Science Foundation of China (21676022 & 21706004), and the Fundamental Research Funds for the Central Universities (BHYC1701A).

References

- [1] W. Li, F. Zhang, Y. Dou, Z. Wu, H. Liu, X. Qian, D. Gu, Y. Xia, B. Tu, D. Zhao, *Adv. Energy Mater.* 1 (2011) 382-386.
- [2] Y. Zhang, S. J. Park, *Carbon* 122 (2017) 287-297.
- [3] S. Guo, Y. Zhu, Y. Yan, Y. Min, J. Fan, Q. Xu, H. Yun, *J. Power Sources* 316 (2016) 176-182.
- [4] T. Li, W. Zhang, L. Zhi, H. Yu, L. Dang, F. Shi, H. Xu, F. Hu, Z. Liu, *Nano Energy* 30 (2016) 9-17.
- [5] L. F. Que, F. D. Yu, Z. B. Wang, D. M. Gu, *Small* 14 (2018) 1704508.
- [6] W. Lu, M. Sevilla, A. B. Fuertes, M. Robert, Y. Gleb, *Adv. Funct. Mater.* 22 (2012) 827-834.

- 1 [7] C. Zheng, X. Zhou, H. Cao, G. Wang, Z. Liu, J. Power Sources 258 (2014) 290-296.
- 2 [8] Z. Yang, J. Zhang, M. C. Kintner–Meyer, X. Lu, D. Choi, J.P. Lemmon, J. Liu, Chem.
- 3
- 4 Rev. 111 (2011) 3577-3613.
- 5
- 6 [9] S. Kondrat, C.R. Pérez, V. Presser, Y. Gogotsi, A. A. Kornyshev, Energ. Environ. Sci. 5
- 7
- 8 (2012) 6474-6479.
- 9
- 10 [10] Q. Lu, Y. Chen, W. Li, J. Chen, J. Xiao, F. Jiao, J. Mater. Chem. A 1 (2013) 2331- 2336.
- 11
- 12 [11] L. F. Que, F. D. Yu, K. W. He, Z. B. Wang, D. M. Gu, Chem. Mater. 29 (2017) 9133-
- 13
- 14 9141.
- 15
- 16 [12] L. Chen, T. Ji, L. Brisbin, J. Zhu, ACS Appl. Mater. Inter. 7 (2015) 12230–12237
- 17
- 18 [13] K. Wang, Y. Cao, X. Wang, Q. Fan, W. Gibbons, T. Johnson, B. Luo, Z. Gu, Energy 94
- 19
- 20 (2016) 666-671.
- 21
- 22 [14] L. F. Que, F. Yu, L. Zheng, Z. Wang, D. Gu, Nano Energy 45 (2018) 337-345.
- 23
- 24 [15] C. Choi, J. A. Lee, A. Y. Choi, Y. T. Kim, X. Lepro, M.D. Lima, R. H. Baughman, S. J.
- 25
- 26 Kim, Adv. Mater. 26 (2014) 2059-2065.
- 27
- 28 [16] X. Fan, C. Yu, J. Yang, Z. Ling, C Hu, M. D. Zhang, J Qiu, Adv. Energy Mater. 5 (2015)
- 29
- 30 1401761.
- 31
- 32 [17] M. Sevilla, A. B. Fuertes, ACS Nano 8 (2014) 5069-5078.
- 33
- 34
- 35 [18] S. W. Zhang, B. S. Yin, C. Liu, Z. B. Wang, D. M. Gu, Chem. Eng. J. 349 (2018) 509-
- 36
- 37 521.
- 38
- 39 [19] S. Yang, X. Feng, X. Wang, K. Müllen, Angew. Chem. Int. Ed. 50 (2011) 5339-5343.
- 40
- 41 [20] R. Menzel, S. Barg, M. Miranda, D. B. Anthony, S. M. Bawaked, M. Mokhtar, S. A. Al–
- 42
- 43 Thabaiti, S. N. Basahel, E. Saiz, M. S. P. Shaffer, Adv. Funct. Mater. 25 (2015) 28-35.
- 44
- 45 [21] X. Yu, J. Zhao, R. Lv, Q. Liang, C. Zhan, Y. Bai, Z. Huang, W. Shen, F. Kang, J. Mater.
- 46
- 47 Chem. A 3 (2015) 18400-18405.
- 48
- 49
- 50
- 51
- 52
- 53
- 54
- 55
- 56
- 57
- 58
- 59
- 60
- 61
- 62
- 63
- 64
- 65

- 1 [22] D. Feng, T. Lei, M. R. Lukatskaya, J. Park, Z. Huang, M. Lee, L. Shaw, S. Chen, A. A.
2 Yakovenko, A. Kulkarni, J. Xiao, K. Fredrickson, J. B. Tok, X. Zou, Y. Cui, Z. Bao. *Nat.*
3 *Energy*. 3 (2018) 30-36.
4
5
6
7 [23] H. B. Wu, X. W. Lou. *Sci. Adv.* 3 (2017) eaap9252.
8
9
10 [24] D. Dong, H. Guo, G. Li, L. Yan, X. Zhang, W. Song, *Nano Energy* 39 (2017) 470-477.
11
12 [25] D. Sheberla, J. C. Bachman, J. S. Elias, C. Sun, Y. S. Horn, M. Dinca, *Nat. Mat.* 16
13 (2017) 220-224.
14
15
16 [26] H. Sun, L. Mei, J. Liang, Z. Zhao, C. Lee, H. Fei, M. Ding, J. Lau, M Li, C. Wang, X.
17 Xu, G. Hao, B. Papandrea, I. Shakir, B. Dunn, Y. Huang, X. Duan, *Science*, 356 (2017)
18 599-604.
19
20
21
22
23 [27] Y. Zhao, L. Goncharova, Q. Zhang, P. Kaghazchi, Q. Sun, A. Lushington, B. Wang, R.
24 Li, X. Sun, *Nano Lett.* 17 (2017) 5653-5659.
25
26
27
28 [28] P. Zhang, B. Y. Guan, L. Yu, X. W. Lou. *Angew Chem. Int. Ed.* 56 (2017) 7141-7145.
29
30
31 [29] N. Cheng, S. Stambula, D. Wang, M. Banis, J. Liu, A. Riese, B. Xiao, R. Li, T.-K. Sham,
32 L. Liu, G. Botton and X. Sun, *Nat. Commun.* 7 (2016) 13638.
33
34
35 [30] K. Kaliyappan, J. Liu, B. Xiao, A. Lushington, R. Li, T. K. Sham, and X. Sun, *Adv.*
36 *Funct. Mater.* 27 (2017)1701870.
37
38
39
40
41 [31] C. Qu, Y. Jiao, B. Zhao, D. Chen, R. Zou, K.S. Walton, M. Liu, *Nano Energy* 26 (2016)
42 66-73.
43
44
45
46 [32] S. Osman, R. A. Senthil, J. Pan, W. Li, *J. Power Sources* 391 (2018) 162-169.
47
48 [33] L. Xin, Q. Liu, J. Liu, R. Chen, R. Li, Z. Li, J. Wang, *Electrochim. Acta* 248 (2017) 215-
49 224.
50
51
52
53 [34] X. Yan, X. Li, Z. Yan, *Appl. Surf. Sci.* 308 (2014) 306-310.
54
55
56 [35] Y. Chen, D. Ni, X. Yang, C. Liu, J. Yin, K. Cai, *Electrochim. Acta* 278 (2018) 114-123.
57
58 [36] S. Sundriyal, H. Kaur, S.K. Bhardwaj, S. Mishra, K.-H. Kim, A. Deep, *Coord. Chem.*
59 *Rev.*, 369 (2018) 15-38
60
61
62
63
64
65

- 1
2
3
4
5
6
7
8
9
10
11
12
13
14
15
16
17
18
19
20
21
22
23
24
25
26
27
28
29
30
31
32
33
34
35
36
37
38
39
40
41
42
43
44
45
46
47
48
49
50
51
52
53
54
55
56
57
58
59
60
61
62
63
64
65
- [37] J. Zhang, J. Xue, P. Li, S. Huang, H. Feng, H. Luo, *Electrochim. Acta* 284 (2018) 328-335.
- [38] Y. Liu, J. Xu, S. Liu, *Microporous Mesoporous Mater.* 236 (2016) 94-99.
- [39] Y. Yang, S. Hao, H. Zhao, Y. Wang, X. Zhang, *Electrochim. Acta* 180 (2015) 651-657.
- [40] S. Zhang, X. Shi, D. Moszynski, T. Tang, P.K. Chu, X. Chen, E. Mijowska, *Electrochim. Acta* 269 (2018) 580-589.
- [41] B. Xiao, B. Wang, J. Liu, K. Karthikeyan, Q. Sun, Y. Liu, G. Dadheech, M. Balogh, L. Yang, T.-K. Sham, R. Li, M. Cai and X. Sun, *Nano Energy* 34 (2017) 120-130.
- [42] R. Bendi, V. Kumar, V. Bhavanasi, K. Parida, P. S. Lee, *Adv. Energy Mater.* 6 (2016) 1501833.
- [43] M. Yu, L. Zhang, X. He, H. Yu, J. Han, M. Wu, *Mater. Lett.* 172 (2016) 81-84
- [44] B. Gao, Y. Ma, J. Mei, S. Lu, L. Ren, *Chem. Eng. J.* 331 (2018) 597-605.
- [45] N. Zhang, X. Yang, X. Yu, Y. Jia, J. Wang, L. Kong, Z. Jin, B. Sun, T. Luo, J. Liu, *Chem. Eng. J* 252 (2014) 220-229.
- [46] W. Bao, A. K. Mondal, J. Xu, C. Wang, D. Su, G. Wang, *J. Power Sources* 325 (2016) 286-291.
- [47] J. A. Carrasco, J. Romero, G. Abellan, J. Hernandez-Saz, S. I. Molina, C. Marti-Gastaldo, E. Coronado, *Chem. Commun.* 52 (2016) 9141-9144.
- [48] X. He, H. Zhang, H. Zhang, X. Li, N. Xiao, J. Qiu, *J. Mater. Chem. A* 2014, 2, 19633.
- [49] P. Zhang, F. Sun, Z. Shen, D. Cao, *J. Mater. Chem. A* 2 (2014) 12873-12880.
- [50] Y. Pan, Y. Zhao, S. Mu, Y. Wang, C. Jiang, Q. Liu, Q. Fang, M. Xue, S. Qiu, *J. Mater. Chem. A* 5 (2017) 9544-9552.
- [51] X. Chen, Y. He, H. Song, Z. Zhang, *Carbon* 72 (2014) 410-420.
- [52] I. A. Khan, A. Badshah, I. Khan, D. Zhao, M.A. Nadeem, *Micropor. and Mesopor. Mat.* 253 (2017) 169-176.

- 1
2
3
4
5
6
7
8
9
10
11
12
13
14
15
16
17
18
19
20
21
22
23
24
25
26
27
28
29
30
31
32
33
34
35
36
37
38
39
40
41
42
43
44
45
46
47
48
49
50
51
52
53
54
55
56
57
58
59
60
61
62
63
64
65
- [53] L. Wan, E. Shamsaei, C. D. Easton, D. Yu, Y. Liang, X. Chen, Z. Abbasi, A. Akbari, X. Zhang, H. Wang, *Carbon* 121 (2017) 330-336.
- [54] J. Yang, G. Li, M. Cai, P. Pan, Z. Li, Y. Bao, Z. Chen, *Chem. Commun.* 53 (2017) 5028-5031.
- [55] C. Wang, C. Liu, J. Li, X. Sun, J. Shen, W. Han, L. Wang, *Chem. Commun.* 53 (2017) 1751-1754.
- [56] M. Karnan, K. Subramani, P. K. Srividhya, M. Sathish, *Electrochim. Acta* 228 (2017) 586-596.
- [57] Y. Li, G. Wang, T. Wei, Z. Fan, P. Yan, *Nano Energy* 19 (2016) 165-175.
- [58] K. Song, W. Song, L. Fan, *J. Mater. Chem. A* 3 (2015) 16104-16111.
- [59] L. Hu, X. Peng, Y. Lia, L. Wang, K. Huo, L. Y. S. Lee, K. Wong, P. K. Chub, *Nano Energy* 34 (2017) 515-523.
- [60] Y. Liu, G. Li, Y Guo, Y. Ying, X. Peng, *ACS Appl. Mater. Inter.* 9 (2017) 14043-14050.
- [61] L. Xin, Q. Liu, J. Liu, R. Chen, R. M. Li, Z. Li, J. Wang, *Electrochim. Acta* 248 (2017) 215-224.

Supporting Information

A green and template-free synthesis process of superior carbon material with ellipsoidal structure as enhanced material for supercapacitors

Yanzhi Sun^a, Shicheng Guo^a, Wei Li^b, Junqing Pan^{a,*}, Carlos Fernandez^c, Raja Arumugam Senthil^a, Xueliang Sun^{d,*}

^aState Key Laboratory of Chemical Resource Engineering, Beijing Engineering Center for Hierarchical Catalysts, Beijing Advanced Innovation Center for Soft Matter Science and Engineering, Beijing University of Chemical Technology, Beijing 100029, China

^bDepartment of Engineering Technology and Texas Center for Superconductivity, University of Houston, Houston, TX 77204, USA

^cSchool of Pharmacy and Life Sciences, Robert Gordon University, Aberdeen, AB10 7GJ, UK

^dDepartment of Mechanical and Materials Engineering, University of Western Ontario, London, ON N6A 5B9, Canada

* Corresponding author: Tel./Fax: +86-10-64448461 (J. Pan)

E-mails: jqpan@mail.buct.edu.cn (Junqing Pan) & xsun9@uwo.ca (Xueliang Sun)

Supplementary figures

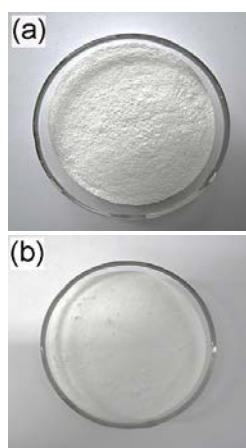


Fig. S1 Photographs of the obtained Al(OH)₃ (a) before and (b) after Bayer cycle.

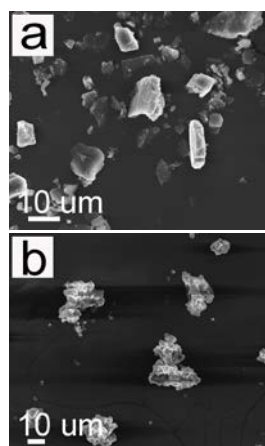


Fig. S2 SEM images of the obtained $\text{Al}(\text{OH})_3$, (a) before and (b) after Bayer cycle.

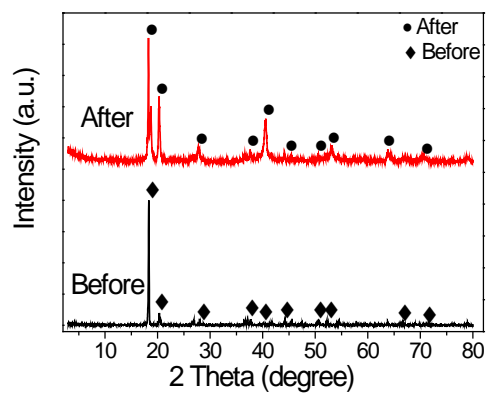


Fig. S3 XRD patterns of the obtained Al(OH)₃ before and after Bayer cycle.

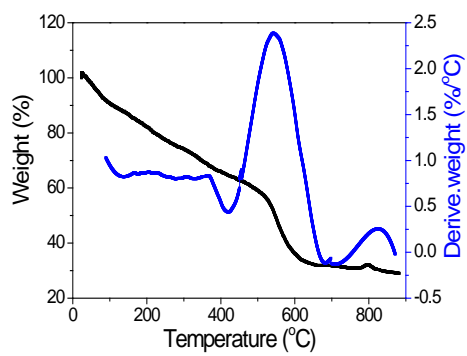


Fig. S4 TGA curve of the obtained Al-BTC from 20 to 900 °C at heating rate of 10 °C min⁻¹ in N₂ atmosphere.ss

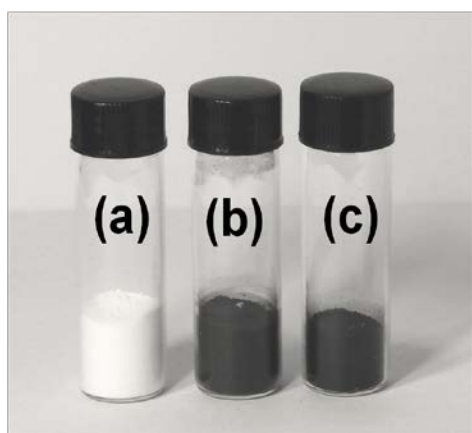


Fig. S5 Photographs of the obtained (a) Al-BTC, (b) C/Al₂O₃ and (c) PC.

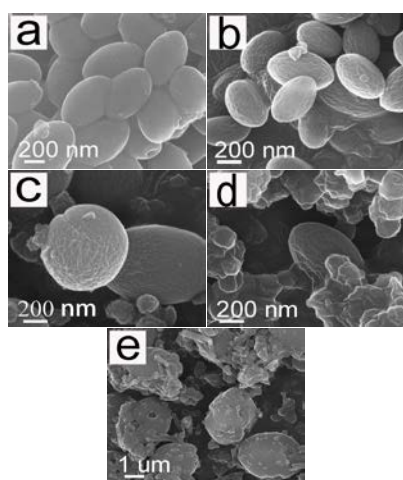


Fig. S6 SEM images of obtained Al-BTC for different reaction times of (a) 8 h, (b) 9 h, (c) 10 h, (d) 11 h and (e) 12 h.

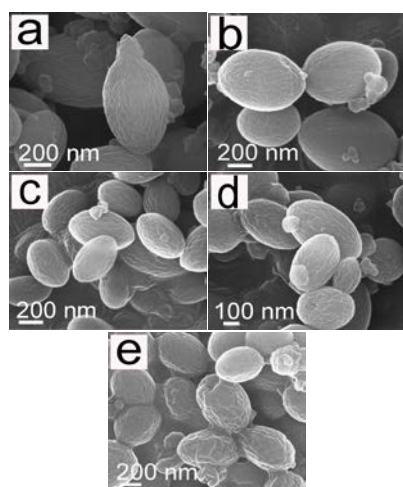


Fig. S7 SEM images of obtained Al-BTC at different temperatures of (a) 100 °C, (b) 110 °C, (c) 120 °C, (d) 130 °C and (e) 140 °C.

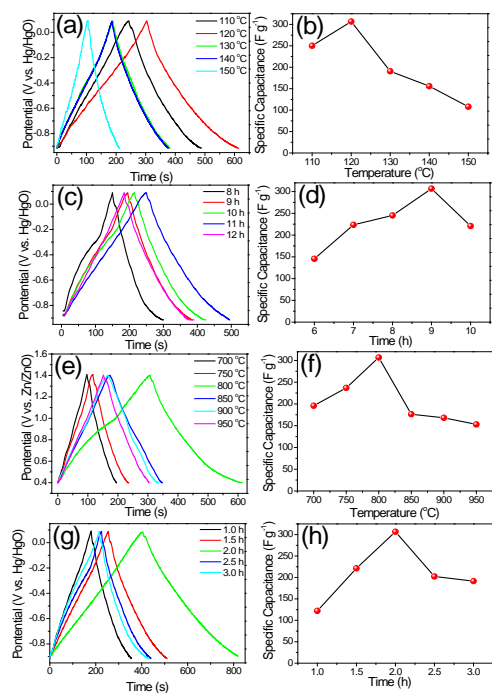


Fig. S8 GCD curves and specific capacitance of PC obtained at (a,b) different synthesized temperature from 110-150 °C, (c,d) different synthesized time from 6-10 h, (e,f) different carbonization temperature from 700-950 °C and (g,h) different carbonization time from 1-3 h of Al-BTC at current density of 1 A g⁻¹ in 6 M KOH.

Supplementary tables

Table S1 Comparison of specific capacitance of the obtained PC with the some carbons reported in the literatures.

References	Electrolyte	Specific capacitance at 1 A g ⁻¹
This work	6 M KOH	306.4 F g ⁻¹
Ref.33	6 M KOH	245 F g ⁻¹
Ref.34	6 M KOH	173.6 F g ⁻¹
Ref.37	6 M KOH	211 F g ⁻¹
Ref.38	6 M KOH	88 F g ⁻¹
Ref.39	6 M KOH	170 F g ⁻¹
Ref.40	6 M KOH	249 F g ⁻¹
Ref.49	6 M KOH	293 F g ⁻¹
Ref.50	6 M KOH	290 F g ⁻¹
Ref.51	6 M KOH	270 F g ⁻¹
Ref.52	6 M KOH	275 F g ⁻¹
Ref.53	6 M KOH	219.41 F g ⁻¹
Ref.54	6 M KOH	253.6 F g ⁻¹
Ref.55	6 M KOH	300 F g ⁻¹
Ref.56	6 M KOH	240 F g ⁻¹